# Loss-on-Drying Prediction for a Vibrated Fluidised Bed Dryer by Means of Mass and Energy Balances

Katharina Kiricenko, Felix Hartmann, Andreas Altmeyer & Peter Kleinebudde

Journal of Pharmaceutical Innovation (2023) 18:2429–2446
https://doi.org/10.1007/s12247-023-09802-w

ORIGINAL ARTICLE

# Loss-on-Drying Prediction for a Vibrated Fluidised Bed Dryer by Means of Mass and Energy Balances

Katharina Kiricenko[1] · Felix Hartmann[2] · Andreas Altmeyer[2] · Peter Kleinebudde[1]

Accepted: 24 November 2023 / Published online: 8 December 2023


## Abstract

**Purpose** Continuous wet granulation and drying require an adequate process control strategy to ensure the product quality. The most important critical quality attributes of dried granules are the granule size distribution and moisture content. Process analytical technologies (PATs) are available for real-time monitoring of moisture content by, e.g., near-infrared spectroscopy (NIRS), which requires additional installation and complex multivariate validation. Thus, a mass and energy balance (MEB) was derived for a vibrated fluidised bed dryer, which is part of the QbCon® 1 intended for continuous wet granulation and drying.

**Method** Process parameters that are frequently logged were used for the derivation of a MEB. The predicted MEB was compared with the measured loss-on-drying (LOD) for two different formulations.

**Results** The model-derived data were in good agreement with the observed LOD, leading to RMSE values of 0.12–0.45.

**Conclusion** The implemented MEB can predict the LOD over time and thus might be suitable as a soft sensor without the installation of additional sensors. The obtained energy flux gives insight into the heat transfer, and the derived energy balance might be used to determine the required energy under certain drying conditions.

**Keywords** Continuous manufacturing · Vibrated fluidised bed dryer · Mass balance · Energy balance · Process monitoring · LOD prediction

## Symbols and Abbreviations

| | |
|---|---|
| $AF_{IN}$ | Inlet air flow |
| $AF_{OUT}$ | Outlet air flow |
| $c_a$ | Specific heat capacity of air |
| $c_{formulation}$ | Specific heat capacity of the formulation |
| CM | Continuous manufacturing |
| $c_{lactose-MCC}$ | Specific heat capacity of the lactose-MCC formulation |
| $c_{mannitol}$ | Specific heat capacity of the mannitol formulation |
| CQA | Critical quality attributes |
| $c_w$ | Specific heat capacity of water |
| $c_{wv}$ | Specific heat capacity of water vapour |
| D | Diameter |
| $\Delta h_v$ | Specific evaporation enthalpy of water |
| DoE | Design of the experiment |
| FBD | Fluidised bed dryer |
| $h_{da}$ | Specific enthalpy of dry air |
| $h_w$ | Specific enthalpy of water vapour |
| KE | Kneading element |
| L/S | Liquid-to-solid |
| LOD | Loss-on-drying |
| $LOD_0$ | Loss-on-drying of starting material |
| LPCE | Long pitch conveying element |
| $M_{air}$ | Molar weight of water |
| MCC | Microcrystalline cellulose |
| $\dot{m}_{da}$ | Mass flow of dry air |
| $\dot{m}_{da-ambient-IN}$ | Mass flow dry air through ambient air entering dryer |
| $\dot{m}_{da-IN}$ | Mass flow of dry air through inlet air |
| $\dot{m}_{da-OUT}$ | Mass flow of dry air through outlet air |

✉ Peter Kleinebudde
kleinebudde@hhu.de

1 Faculty of Mathematics and Natural Sciences, Institute of Pharmaceutics and Biopharmaceutics, Heinrich Heine University Dusseldorf, Universitaetsstrasse 1, 40225 Dusseldorf, Germany

2 L.B. Bohle Maschinen und Verfahren GmbH, 59320 Ennigerloh, Germany

| | |
|---|---|
| MEB | Mass and energy balance |
| $\dot{m}_{solid-IN}$ | Mass flow of dry powder entering dryer |
| $\dot{m}_{solid-loss-OUT}$ | Mass flow of dry powder lost through filter |
| $\dot{m}_{solid-OUT}$ | Mass flow of dried granules leaving dryer |
| $\dot{m}_{w}$ | Mass flow of water |
| $\dot{m}_{wa}$ | Mass flow of wet air |
| $\dot{m}_{wa-IN}$ | Mass flow of wet air through inlet air |
| $\dot{m}_{w-ambient-IN}$ | Mass flow of water through ambient air |
| $\dot{m}_{wa-OUT}$ | Mass flow of wet air through outlet air |
| $M_{water}$ | Molar weight of water |
| $\dot{m}_{w-corr.}$ | Difference in water mass flow between entering and leaving air in empty state |
| $\dot{m}_{w-evap-OUT}$ | Mass flow of evaporated water |
| $\dot{m}_{w-granules-IN}$ | Mass flow of water through granules entering dryer |
| $\dot{m}_{w-granules-loss-OUT}$ | Mass flow of water through granules lost through filter |
| $\dot{m}_{w-granules-OUT}$ | Mass flow of water through dried granules |
| $\dot{m}_{w-IN}$ | Mass flow of water through inlet air |
| $\dot{m}_{w-OUT}$ | Mass flow of water through outlet |
| N | Number of measurement points |
| NIRS | Near-infrared spectroscopy |
| O | Observed LOD |
| $p$ | Pressure |
| P | Predicted LOD |
| $p_{ambient}$ | Pressure of ambient air |
| PAT | Process analytical technology |
| $\varphi$ | Relative humidity |
| $\varphi_{ambient}$ | Relative humidity of ambient air |
| $\varphi_{IN}$ | Relative humidity of inlet air |
| $\varphi_{OUT}$ | Relative humidity of outlet air |
| $p_{IN}$ | Pressure of inlet air |
| $p_{norm}$ | Normalised pressure |
| $p_{OUT}$ | Pressure of outlet air |
| $p_s$ | Saturation vapour pressure |
| $p_{wv}$ | Partial pressure of water vapour |
| $\dot{Q}$ | Energy flux |
| $\dot{Q}_{air-ambient-IN}$ | Energy flux of ambient air |
| $\dot{Q}_{air-IN}$ | Energy flux of inlet air |
| $\dot{Q}_{air-OUT}$ | Energy flux of outlet air |
| $\dot{Q}_{conduction-OUT}$ | Heat loss due to conduction |
| $\dot{Q}_{evaporation-OUT}$ | Heat loss due to evaporation |
| $\dot{Q}_{granules-IN}$ | Energy flux of granules |
| $\dot{Q}_{IN}$ | Sum of entering energy flux |
| $\dot{Q}_{loss}$ | Heat loss |
| $\dot{Q}_{OUT}$ | Sum of leaving energy flux |
| $R_{da}$ | Specific gas constant of dry air |
| $\rho_{wa}$ | Density of wet air |
| $\rho_{wa-IN}$ | Density of wet air of inlet air |
| $\rho_{wa-OUT}$ | Density of wet air of outlet air |
| RMSE | Root mean square error |
| $R_w$ | Specific gas constant of water vapour |
| $R_{wa}$ | Specific gas constant of wet air |
| $S\dot{F}R$ | Solid feed rate |
| $T$ | Temperature |
| $T_{ambient}$ | Temperature of ambient air |
| $T_{barrel3}$ | Barrel temperature at the third position |
| $T_{compressedair}$ | Temperature of compressed air |
| $T_{granules}$ | Temperature of granules |
| $T_{IN}$ | Drying temperature |
| $T_{norm}$ | Normalised temperature |
| $T_{OUT}$ | Outlet air temperature directly after the drying chamber |
| $T_{OUT2}$ | Outlet air temperature |
| TSG | Twin-screw wet granules |
| $T_{SIEV}$ | Temperature inside drying chamber |
| $T_{tr}$ | Triple point temperature of water |
| $u_i$ | Measurement uncertainty of different variables $x_i$ |
| $u_y$ | Measurement uncertainty of variable $y$ |
| VFBD | Vibrating fluidised bed dryer |
| $Vib$ | Vibration acceleration |
| $\dot{V}_{IN}$ | Volume flow of inlet air |
| $\dot{V}_{norm}$ | Normalised air flow |
| $\dot{V}_{OUT}$ | Volume flow of outlet air |
| $X$ | Absolute humidity |
| $X_{ambient}$ | Absolute humidity of ambient air |
| $X_{IN}$ | Absolute humidity of inlet air |
| $X_{OUT}$ | Absolute humidity of outlet air |

## Introduction

Twin-screw wet granulation (TSG) has been extensively studied recently [1–7]. Granule properties can be modified via TSG by changing the powder feed rate [6, 8], liquid-to-solid (L/S) ratio [9, 10], screw speed [8, 11] or screw configuration [3, 12]. Since process manufacturing is changing from traditional batch manufacturing to continuous manufacturing (CM), TSG enables the continuous production of granules. Smaller equipment footprint [2], less waste production [13], better control of product quality [14] and real-time release [13] are some of the advantages of CM. Further processing of the produced granules, e.g. tableting, requires an initial drying step.

There are several dryer types that can be implemented after TSG into a single CM line. A segmented fluidised bed dryer (FBD) is a common method for performing drying semi-continuously. Moreover, CM lines with 6 [15] or 10 [16] segmented drying chambers are well established by the GEA Group (ConsiGma™) [17] and Glatt (ModCos) [18]. A horizontal FBD with a screw conveyer inside the drying chamber was introduced by the company Lödige Process Technology (GRANUCON®) [19]. Inspired by the food industry, where vibrating FBDs (VFBDs) are commonly used, this type is also implemented into a CM line by L.B. Bohle Maschinen und Verfahren (QbCon®) [20, 21]. A CM line from "powder to tablet" via wet granulation and intermediate drying requires an adequate control strategy to ensure product quality [22]. One critical quality attribute (CQA) that needs to be considered is granule moisture, called loss-on-drying (LOD) [22].

Process analytical technologies (PATs) allow real-time monitoring of CQAs such as LOD. Therefore, microwave resonance technology [23], NIRS [24] or Raman spectroscopy [25] is widely used. A disadvantage of these methods is the implementation and validation of an additional sensor [24]. Another approach based on thermodynamics is the calculation using the mass and energy balance (MEB) for real-time LOD control. For the implementation of MEB, a further sensor installation is not necessary as it is based on the already included standard sensors that continuously log process values such as relative humidity, temperature, pressure and air flow of the inlet and outlet air. Regarding dryers intended or implemented for the CM line, the derivation of a MEB was already investigated for the GPCG2 FBD with 10 segments including the usage of NIRS with good prediction of the LOD [24]. In addition, for the 6-segmented FBD of ConsiGma™, a MEB was examined [26] compared to PAT by Raman as well as NIRS [25], which provided good correlations. Mathematical modelling enables the prediction of LOD and was previously introduced for drying via FBD [27] or VFBD [28] in the food industry. In the pharmaceutical field, a mathematical model was investigated for horizontal FBD combined with a screw conveyor using drying kinetics for the prediction of LOD [29]. In addition, for the FBD of ConsiGma™, a process model was established as a soft sensor [30] as well as mechanistic modelling for the simulation of LOD at different granule size fractions [31]. A combination of a data-driven technique using a latent-variable model and a knowledge-driven mechanic model applied for a segmented FBD. Thereby, fault detection and cause detection were obtained [32]. For the VFBD grey box modelling [33], flowsheet simulation [34] and a one-dimensional plug flow model [35] were constructed.

The aim of the present work is the stepwise derivation of a MEB for the continuous VFBD of QbCon® 1 using logged process values of the sensors installed in the drying and granulation unit. This offers the first step toward the development of an orthogonal method, which might be used additional to another PAT method. The applicability of the set MEB to predict the LOD of two different formulations at different LOD ranges was investigated as well for gain insights into the energy flux during heating and drying.

## Materials and Methods

### Materials

Two formulations were applied for wet granulation and drying, which contained either 97% (w/w) mannitol (Pearlitol 200 SD, Roquette, Lestrem, France) or 80% (w/w) alpha-lactose monohydrate (Granulac® 200, MEGGLE GmbH & Co. KG, Wasserburg am Inn, Germany) and 17% (w/w) microcrystalline cellulose (MCC, VIVAPUR® 101, JRS PHARMA GmbH & Co. KG, Rosenberg, Germany). 3% (w/w) polyvinylpyrrolidone K 30 (Kollidon® 30, BASF SE, Ludwigshafen, Germany) was used as binder in both formulations. Demineralized water served as the granulation liquid.

### Preparation of the Powder Mixtures

The mixtures were blended in 5 kg batches for 20 min at 25 rpm in a laboratory-scale blender (LM 40, L. B. Bohle Maschinen und Verfahren GmbH, Ennigerloh, Germany).

### Twin-Screw Wet Granulation and Drying

Continuous wet granulation and drying are performed using QbCon® 1 (L.B. Bohle Maschinen und Verfahren GmbH, Ennigerloh, Germany) comprising a feeding unit, a twin-screw wet granulator and a continuous vibrated fluidised bed dryer. For granulation, a screw diameter (D) of 16 mm and a total screw length of $20.15 \times D$ were set. The screw configuration contained long pitch conveying elements (LPCE), short pitch conveying elements (SPCE) and kneading elements (KE) with a stagger angle of 60°. The following screw configuration was used from inlet to the outlet: 4D LPCE–3.75D SPCE–1.2D (6) KE–5D SPCE–1.2D (6) KE–5D SP CE. A gravimetric feeder (DIW-PE-GZD-P 150.12 Gericke AG, Regensdorf, Switzerland) was used to feed the powder blend and the granulation liquid was fed via a micro-gear pump (MZR-7205, HNO-Mikrosysteme GmbH, Schwerin, Germany) with a nozzle diameter of 0.12 mm. The liquid port was set before the first kneading block. Solid feed rate ($\dot{SFR}$) of 1.2 kg/h, screw speed of 100 rpm, L/S ratio of 0.15 (mannitol formulation) or 0.20 (lactose-MCC formulation) and barrel temperature of 25 °C were kept constant for all

**Table 1** Drying conditions using mannitol (M) and lactose-MCC (L) as the formulation

| Experiment | $T_{IN}$ [K] | $AF_{IN}$ [$Nm^3$] | Vib [$m/s^2$] |
|---|---|---|---|
| ***M*1** | 321.15 | 12 | 4.5 |
| ***M*2** | 321.15 | 18 | 7.5 |
| ***M*3** | 333.15 | 15 | 6 |
| ***L*1** | 321.15 | 18 | 7.5 |
| ***L*2** | 333.15 | 15 | 6 |
| ***L*3** | 345.15 | 18 | 7.5 |

experiments. After reaching a uniform torque fluctuation in the TSG process, the granules were supplied to the drying chamber. The dryer was preheated for each drying condition for 1 h. The process was run for 1 h under constant granulation and drying parameters. In total, 3 different drying conditions were selected from a previous publication [21] for each formulation to obtain different LOD ranges. Therefore, different parameter settings for the drying temperature ($T_{IN}$), inlet air flow ($AF_{IN}$) and vibration acceleration (*Vib*) were used. Mannitol and lactose-MCC granules were dried as listed in Table 1. Samples of dried granules were taken every 5 min and stored in glass containers sealed from air until the LOD was measured in triplicate. The inlet and exhaust air humidity, temperature, air flow and pressures were recorded internally by the sensors installed in the equipment. The ambient relative humidity ($\varphi_{ambient}$) and temperature ($T_{ambient}$) were noticed every 30 min using wireless temperature and humidity sensor testo 175 H1 (Testo SE &Co. KGaA, Titisee-Neustadt, Germany). The $\varphi_{ambient}$ was converted further into absolute humidity ($X_{ambient}$).

MEB was derived stepwise using an additional run for lactose-MCC with the previously described granulation parameters. For this, a heating phase of 80 min in an empty dryer was investigated and the granulation and drying were conducted over 150 min. The LOD was determined every 5 min with $n = 1$. Granules were dried at 321.15 K with an $AF_{IN}$ of 18 $Nm^3/h$ and 7.5 $m/s^2$ as *Vib* (*L*1 according to Table 1).

## Design of Experiment—Empty Dryer

In a previous study, the recorded temperatures inside the empty drying chamber were lower than the set $T_{IN}$. [21]. In addition, the outlet temperature ($T_{OUT}$) was lower because of the heat conduction of the stainless steel drying chamber, which led to thermal energy loss [21]. The approach of investigating empty dryers using a design of experiment (DoE) was already introduced by Pauli et al. [24] and was implemented for the MEB of the VFBD. A central composite circumscribed DoE was conducted using $T_{IN}$ (313.25–353.05 K) and $AF_{IN}$ (10.1–19.9 $Nm^3/h$) as factors. The DoE setup is listed in Table 2. The distance between the center and star points $\alpha$ according to Myers et al. is 1.414 to obtain a rotatable and orthogonal design [36]. Thus, a total of 11 experiments were performed involving a center point conducted three times in randomised order. The DoE was built and analysed using MODDE (V13.0, Sartorius Stedim Data Analytics AB, Malmö, Sweden).

The dryer was initially preheated at the beginning of each day for 30 min. Each run was performed for 2 h. For evaluation, only the mean of the last 10 min was used. To monitor the temperature and humidity along the drying chamber, 12 wireless temperature and humidity sensors (RHTemp 1000Ex, MadgeTech Inc., Warner, USA) were used. A detailed description of the position of the sensors inside the dryer can be found in a previous study [21]. Therefore, the temperature inside the drying chamber recorded at position 4 ($T_{SIEV}$), which is close to the inlet of the hot air, was used as the response for this DoE. $T_{OUT}$ is measured directly at the outlet of the drying chamber and was also investigated as response. Figure 1 shows the locations of the investigated sensors used in the DoE.

## Calculation of Absolute Humidity

The measured relative humidity was converted into the absolute humidity mixing ratio $X$ according to Eq. (1) [37].

$$X\left[\frac{g}{kg}\right] = \frac{M_{water}}{M_{air}} * \frac{p_{wv}}{\left(p - p_{wv}\right)} * 1000 \tag{1}$$

$M_{Water}$ and $M_{Air}$ are the molar weights of water and air, $p_{wv}$ describes the partial pressure of water vapour and $p$ the pressure.

**Table 2** CCC-DoE setup with coded and uncoded factors in an empty drying chamber

| *N*° | Factors (coded) | |
|---|---|---|
| | $AF_{IN}$ [$Nm^3/h$] | *DT* [K] |
| 1 | 11.5 (−1) | 319.05 (−1) |
| 2 | 18.5 (+1) | 319.05 (−1) |
| 3 | 11.5 (−1) | 347.25 (+1) |
| 4 | 18.5 (+1) | 347.25 (+1) |
| 5 | 10.1 (−1.414) | 333.15 (0) |
| 6 | 19.9 (+1.414) | 333.15 (0) |
| 7 | 15.0 (0) | 313.25 (−1.414) |
| 8 | 15.0 (0) | 353.05 (+1.414) |
| 9 | 15.0 (0) | 333.15 (0) |
| 10 | 15.0 (0) | 333.15 (0) |
| 11 | 15.0 (0) | 333.15 (0) |

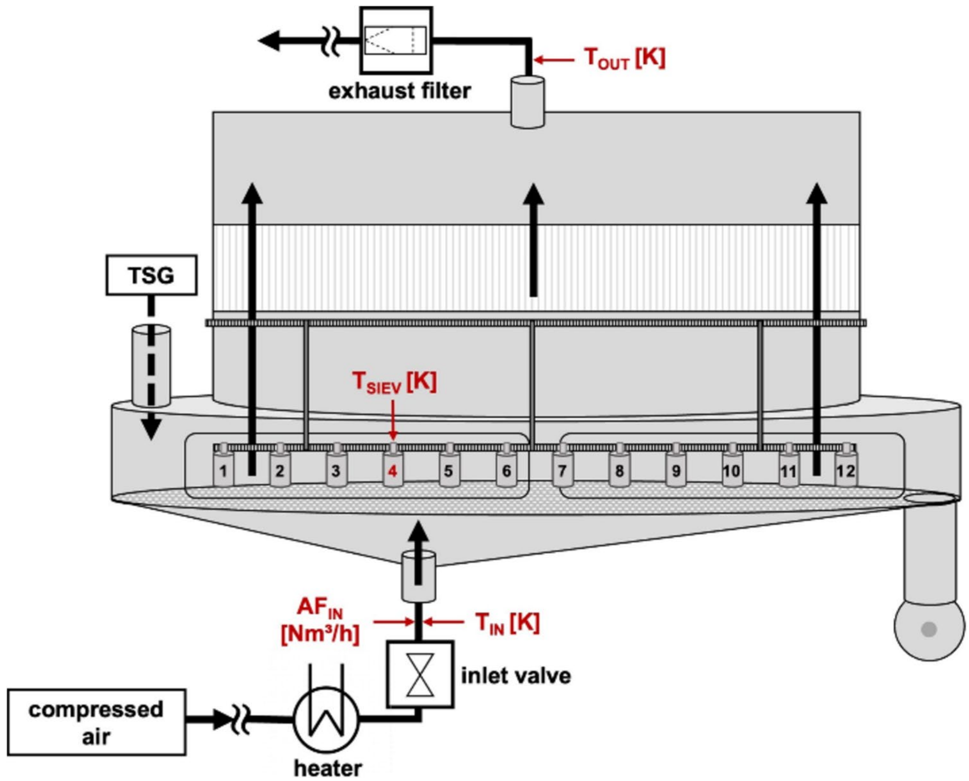


**Fig. 1** Sensor location with investigated factors and response values in the DoE in the empty drying state

## Determination of Water Content (LOD)

Every 5 min, a sample of the dried granules was taken, and the LOD was analysed offline using a moisture analyser (MA 100, Sartorius, Goettingen, Germany). A sample size of approximately 2 g of the dried granules was dried at 80 °C (lactose-MCC formulation) or 105 °C (mannitol formulation). The termination criterion, where the measurement stopped, was set at 0.1% of the mass differences within 150 s. Measurements were performed in triplicates. The LOD of the starting material of each powder composition was also measured in triplicates before granulation and drying of each drying process using a sample size of 4 g.

## LOD Prediction Performance Using Root Mean Square Error

The prediction performance of the LOD using the mass balance was investigated using the root mean square error (RMSE), which was calculated according to Eq. (2) [38]. The RMSE describes the average difference between the predicted LOD ($P$) and the observed LOD ($O$). Therefore, $N$ displays the number of measurement points using $N = 12$ for all experiments.

$$RMSE = \sqrt{\frac{1}{N}\sum_{i=1}^{N}(P_i - O_i)^2} \tag{2}$$

## Propagation of Uncertainty

The *Law of Propagation of Uncertainty* is used to calculate the measurement uncertainty $u_y$ of a variable $y$ subject to measurement uncertainties $u_i$ of different variables $x_i$ and where $f(x_i)$ is the functional relationship between $y$ and $x_i$. The measurement uncertainty $u_y$ can be calculated according to Eq. (3) [39].

$$u_y = \sqrt{\sum_i \left(\frac{\partial f}{\partial x_i} \cdot u_i\right)^2} \tag{3}$$

The uncertainty in $y$ can be presented as the range of reliability according to Eq. (4) [39]. In the following work, $u_y$ is labelled as uncertainty.

$$y = f(x_i) \pm u_y \tag{4}$$

**Table 3** Observed responses of DoE in an empty dryer

| N° | Responses | |
|---|---|---|
| | $T_{SIEV}$ ($T_{granules}$) [K] | $T_{OUT}$[K] |
| 1 | 317.21 | 306.14 |
| 2 | 318.08 | 308.55 |
| 3 | 342.58 | 317.39 |
| 4 | 344.15 | 322.39 |
| 5 | 329.66 | 311.43 |
| 6 | 331.39 | 316.50 |
| 7 | 312.26 | 303.83 |
| 8 | 347.77 | 321.85 |
| 9 | 330.53 | 313.10 |
| 10 | 330.40 | 314.29 |
| 11 | 330.25 | 312.89 |

### Differential Scanning Calorimetry

Differential scanning calorimetry measurements were conducted using a 1 STAR$^e$ system (Mettler-Toledo GmbH, Gießen, Germany). Samples pf 3–5 mg were weighed into sealed aluminium pans and heated from 0 to 260 °C (lactose-MCC formulation) or to 220 °C (mannitol formulation) at a rate of 10 °C/min.

## Results and Discussion

### Investigation of Empty Dryer

A previous study showed a difference between the set $T_{IN}$ and $T_{OUT}$ in empty state [21]. As the stainless-steel dryer and sieve bottom are heated, there is a loss in thermal energy due to heat conduction. This loss of thermal energy is not associated with the evaporation of water during drying. Therefore, a model for $T_{SIEV}$ was set up from the DoE in the empty state. Table 3 gives an overview of the observed responses used to build the following model. Correlating $T_{SIEV}$ against $AF_{IN}$ and $T_{OUT}$ enables the prediction of the conductive energy loss between $T_{SIEV}$ and $T_{OUT}$. According to Pauli et al. [24], the predicted $T_{SIEV}$ based on $AF_{IN}$ and $T_{OUT}$ equals the theoretical granule temperature ($T_{granules}$) as predicted by the temperature of the air that leaves the sieve bottom. Thus, in empty state, the $T_{SIEV}$ ideally equals $T_{IN}$ as well as $T_{OUT}$. During drying of granules, the $T_{IN}$ is higher than $T_{OUT}$ and consequently $T_{SIEV}$ or $T_{granules}$. Hence, the observed response $T_{OUT}$ was applied as a factor for predicting $T_{SIEV}$ as this temperature is closer to $T_{granules}$ due to evaporation compared to $T_{IN}$. Figure 2 displays the evaluation of the set model for predicting $T_{granules}$ using a summary of fit. $R^2$, which is a measure of fit, and $Q^2$, which is the prediction ability, were close to 1.0 (> 0.98). The high value in reproducibility resulted in lower model validity. The observed versus predicted values using the model are also shown in Fig. 2. Equation (5) was used further in the MEB to predict the $T_{granules}$ at the conducted drying conditions.

$$T_{granules}[\mathrm{K}] = -0.87 * AF_{IN} + 2.00 * T_{OUT} - 282.87 \quad (5)$$

### Derivation of Mass Balance

#### Placement of Sensors

The derivation of MEB is based on the sensors installed in QbCon® 1, which are displayed in Fig. 3. The temperature of the compressed air ($T_{compressedair}$) and relative humidity ($\varphi_{IN}$) is measured before the air is heated to the set $T_{IN}$. $\varphi_{IN}$ is converted into the absolute humidity of the inlet air ($X_{IN}$). Before the hot air enters the drying chamber, the $AF_{IN}$, $T_{IN}$ and inlet pressure ($p_{IN}$) are recorded.

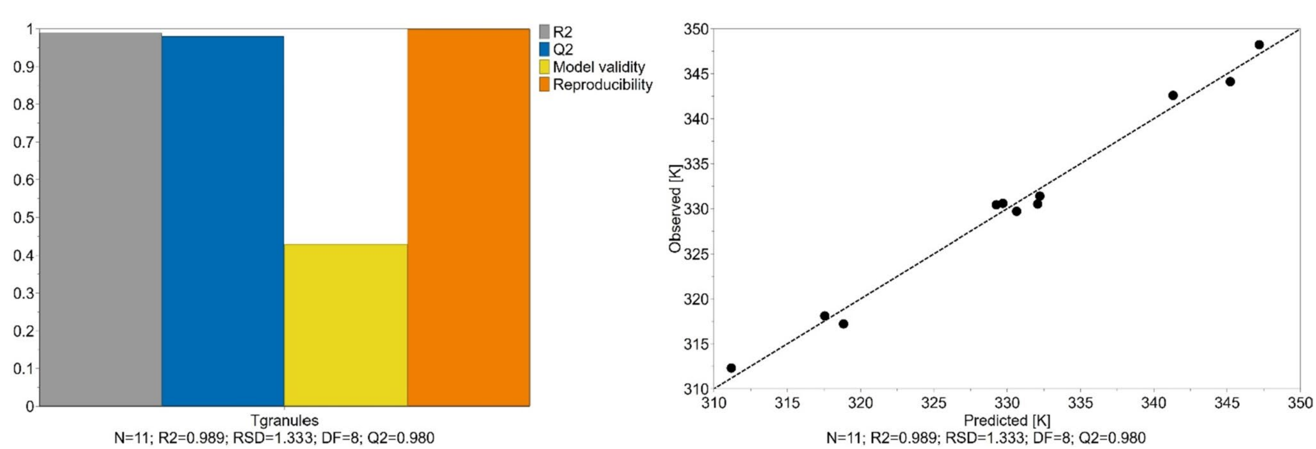


**Fig. 2** Summary of fit and observed versus predicted plot for the model of $T_{granules}$

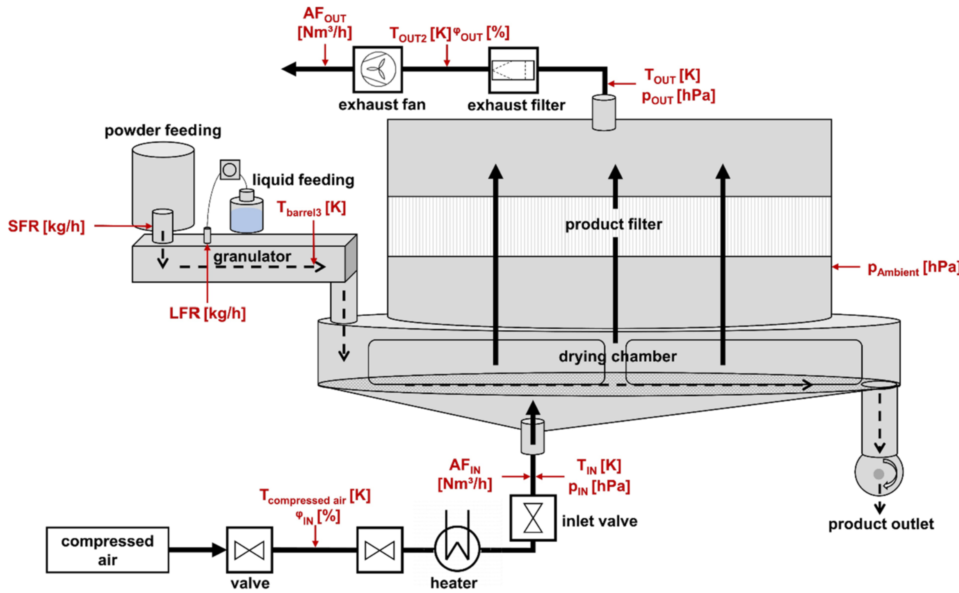


**Fig. 3** Sensor positions of the measured process parameters for the MEB

The ambient pressure ($p_{ambient}$) is recorded by the equipment. Hot and dry air exits the drying chamber by passing through the product filter. At the outlet, the pressure ($p_{OUT}$) and $T_{OUT}$ are measured. After passing the exhaust filter, the outlet temperature ($T_{OUT2}$) and outlet relative humidity ($\varphi_{OUT}$) are recorded and used for the calculation of the absolute humidity ($X_{OUT}$). The outlet air flow ($AF_{OUT}$) is obtained after exiting the exhaust fan. The black arrows represent the flow of air, whereas the dashed arrows show the material flow. During granulation, the $S\dot{F}R$ and liquid feed rate ($L\dot{F}R$) are recorded and the barrel temperature at three positions. The third position ($T_{barrel3}$) was used for the calculations of the energy balance as it is close to the outlet of the TSG and closely represents the temperature of the granules entering the drying chamber.

## Derivation of Mass Balance—Empty Dryer

The mass balance calculation assumed that the amount of mass entering a system equals the amount of mass exiting a system. In the used VFBD, the mass balance was first calculated under empty conditions. Therefore, the water and dry air which enters the drying unit via the inlet air should equal the mass of water and dry air leaving the dryer through the outlet air. Table 4 lists the parameters used to demonstrate the mass balance in the empty state.

$AF_{IN}$ and $AF_{OUT}$ are indicated as the norm volumetric flow ($\dot{V}_{norm}$) for a norm pressure ($p_{norm}$) of 101,325 Pa and norm temperature ($T_{norm}$) of 273.15 K. Therefore, the norm conditions are calculated for the operating volume flow for inlet ($\dot{V}_{IN}$) and outlet air flow ($\dot{V}_{OUT}$) derived from the universal gas equation according to Eq. (6) [40]. Consequently, $\dot{V}_{IN}$ and $\dot{V}_{OUT}$ are calculated as follows:

$$\dot{V}_0\left[\frac{\mathrm{m}^3}{\mathrm{h}}\right] = \frac{p_{norm} * \dot{V}_{norm} * T}{T_{norm} * p} \tag{6}$$

$$\dot{V}_{IN} = \frac{101325\ \mathrm{Pa} * 18.01\frac{\mathrm{m}^3}{\mathrm{h}} * 296.45\ \mathrm{K}}{273.15\ \mathrm{K} * 102780\ \mathrm{Pa}} = 19.27\frac{\mathrm{m}^3}{\mathrm{h}}$$

$$\dot{V}_{OUT} = \frac{101325\ \mathrm{Pa} * 18.22\frac{\mathrm{m}^3}{\mathrm{h}} * 304.75\ \mathrm{K}}{273.15\ \mathrm{K} * 101240\ \mathrm{Pa}} = 20.34\frac{\mathrm{m}^3}{\mathrm{h}}$$

To determine the mass flow of wet air ($\dot{m}_{wa}$) through $\dot{V}_0$, the density of wet air ($\rho_{wa}$) is calculated according to Eq. (7) with

**Table 4** Process parameters used to demonstrate the MEB of derivation at a certain time point in an empty dryer

| Process parameter | Value at *t* |
|---|---|
| $AF_{IN}$ | 18.01 Nm³/h |
| $T_{compressedair}$ | 296.45 K |
| $\varphi_{IN}$ | 5.44% |
| $X_{IN}$ | 0.944 g/kg |
| $p_{IN}$ | 1027.8 hPa |
| $T_{IN}$ | 321.15 K |
| $T_{OUT}$ | 308.85 K |
| $AF_{OUT}$ | 18.22 Nm³/h |
| $T_{OUT}$ | 304.75 K |
| $\varphi_{OUT}$ | 2.43% |
| $X_{OUT2}$ | 0.696 g/kg |
| $p_{OUT}$ | 1012.4 hPa |
| $T_{ambient}$ | 297.35 K |
| $\varphi_{ambient}$ | 40.9% |
| $X_{ambient}$ | 7.67 g/kg |
| $p_{ambient}$ | 1016.0 hPa |

the specific gas constant of wet air ($R_{wa}$) which is calculated using Eq. (8) [40]. Where $R_{da}$ is the specific gas constant of dry air, defined as $287.0\frac{\text{J}}{\text{kg}*\text{K}}$, and $R_w$ of water vapour defined as $461.5\frac{\text{J}}{\text{kg}*\text{K}}$. $\varphi$ is the relative humidity and $p_s$ the saturation vapour pressure.

$$\rho_{wa}\left[\frac{\text{kg}}{\text{m}^3}\right] = \frac{p}{R_{wa} * T} \tag{7}$$

$$R_{wa}\left[\frac{\text{J}}{\text{kg} * \text{K}}\right] = \frac{R_{da}}{1 - \varphi * \frac{p_s}{p} * \left(1 - \frac{R_{da}}{R_w}\right)} \tag{8}$$

Thus, the calculated densities are $1.207\frac{\text{kg}}{\text{m}^3}$ of inlet air ($\rho_{wa-IN}$) and $1.157\frac{\text{kg}}{\text{m}^3}$ of the outlet air ($\rho_{wa-OUT}$). $\dot{m}_{wa}$ of inlet ($\dot{m}_{wa-IN}$) and outlet air ($\dot{m}_{wa-OUT}$) is calculated using Eq. (9):

$$\dot{m}_{wa}\left[\frac{\text{kg}}{\text{h}}\right] = \rho_{wa} * \dot{V}_0 \tag{9}$$

$$\dot{m}_{wa-IN} = 1.207\frac{\text{kg}}{\text{m}^3} * 19.27\frac{\text{m}^3}{\text{h}} = 23.26\frac{\text{kg}}{\text{h}}$$

$$\dot{m}_{wa-OUT} = 1.157\frac{\text{kg}}{\text{m}^3} * 20.34\frac{\text{m}^3}{\text{h}} = 23.53\frac{\text{kg}}{\text{h}}$$

By using $\dot{m}_{wa}$ and $X$, the mass flow of dry air ($\dot{m}_{da}$) and water through the air ($\dot{m}_w$) is calculated using Eqs. (10) and (11):

$$\dot{m}_{da}\left[\frac{\text{kg}}{\text{h}}\right] = \frac{\dot{m}_{wa}}{(1 + X)} \tag{10}$$

$$\dot{m}_{w}\left[\frac{\text{kg}}{\text{h}}\right] = \dot{m}_{da} * X \tag{11}$$

$$\dot{m}_{da-IN} = \frac{23.26\frac{\text{kg}}{\text{h}}}{1 + 0.944 * 10^{-3}\frac{\text{kg}}{\text{kg}}} = 23.24\frac{\text{kg}}{\text{h}}$$

$$\dot{m}_{w-IN} = 23.24\frac{\text{kg}}{\text{h}} * 0.944 * 10^{-3}\frac{\text{kg}}{\text{kg}} = 0.0219\frac{\text{kg}}{\text{h}}$$

$$\dot{m}_{da-OUT} = \frac{23.53\frac{\text{kg}}{\text{h}}}{1 + 0.696 * 10^{-3}\frac{\text{kg}}{\text{kg}}} = 23.51\frac{\text{kg}}{\text{h}}$$

$$\dot{m}_{w-OUT} = 23.51\frac{\text{kg}}{\text{h}} * 0.696 * 10^{-3}\frac{\text{kg}}{\text{kg}} = 0.0164\frac{\text{kg}}{\text{h}}$$

There is a deviation between the incoming and outgoing $\dot{m}_{da}$ and $\dot{m}_w$. $0.0055\frac{\text{kg}}{\text{h}}$ more water enters the drying chamber through the air but not exiting. At the same time, $0.27\frac{\text{kg}}{\text{h}}$ more dry air leaves the system. Vacuum is applied in the drying chamber at the outlet of the TSG and thus ambient air can enter the drying chamber by attraction. In addition, through the rubber seals around the drying chamber, ambient air could have entered, which has a higher relative humidity. Therefore, the assumption was made that the difference between the supply and exhaust dry air is equal to the $\dot{m}_{da}$ from the environment ($\dot{m}_{da-ambient-IN}$). Thus, the $\dot{m}_{da-ambient-IN}$ is determined by converting Eq. (12) and the water entering the drying chamber through the environment ($\dot{m}_{w-ambient-IN}$) is calculated using Eq. (11).

$$\dot{m}_{da-IN} + \dot{m}_{da-ambient-IN} = \dot{m}_{da-OUT} \tag{12}$$

$$\dot{m}_{da-ambient-IN} = 23.51\frac{\text{kg}}{\text{h}} - 23.24\frac{\text{kg}}{\text{h}} = 0.27\frac{\text{kg}}{\text{h}}$$

$$\dot{m}_{w-ambient-IN} = 0.27\frac{\text{kg}}{\text{h}} * 7.67 * 10^{-3}\frac{\text{kg}}{\text{kg}} = 0.0021\frac{\text{kg}}{\text{h}}$$

Despite this, the mass balance of inlet and outlet water is not in balance and due to the ambient air an even higher amount of water entering but not leaving the system. The same phenomenon was observed by Mortier et al. [26] for the investigated datasets using the six segmented FBD of the ConsiGma™ from GEA. The authors had no explanation for the difference in the empty state. Thus, each sensor has an uncertainty that is considered in the calculations as described in the "Propagation of Uncertainty" section. The existing difference in water in the empty state is defined in the following study as $\dot{m}_{w-corr.}$ according to Eq. (13).

$$\dot{m}_{w-corr.} = \left(\dot{m}_{w-IN} + \dot{m}_{W-ambient-IN}\right) - \dot{m}_{w-OUT} \tag{13}$$

For the shown example, the $\dot{m}_{w-corr.}$ corresponds to $0.0076\frac{\text{kg}}{\text{h}}$ and needs to be added to the amount of water leaving through the outlet air ($\dot{m}_{w-OUT}$) while drying the granules for the prediction of the LOD. To determine $\dot{m}_{w-corr.}$, a heating phase before starting the granulation and drying process is required. In contrast to Mortier et al. [26], no correlation was found between the difference in $\dot{m}_w$ and inlet air temperature. The authors used a linear regression with all taken data points and added the "offset" in their publication to the mass balance. With this correlation, they had a good agreement between the measured LOD and the predicted LOD. Figure 4 displays the $\dot{m}_{w-corr.}$ over the time including the sensor uncertainty. Therefore, the heating phase starting from zero is included. Considering the sensor uncertainty, the calculated value covers a large range. As pressurised air is used as inlet air, which cannot be controlled, some fluctuations are possible.

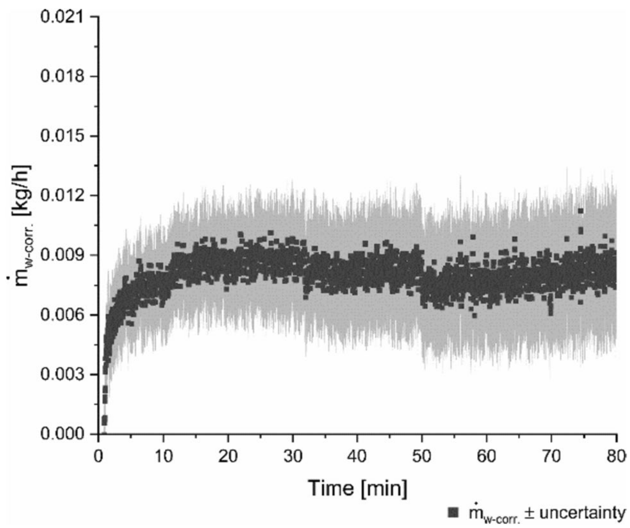


**Fig. 4** Heating phase in empty dryer at 48 °C–18 $Nm^3$/h–7.5 $m/s^2$ over 80 min, $n = 1$ with 4800 measuring points, $\dot{m}_{w-corr}$± uncertainty

### Derivation of Mass Balance—Drying of Granules

The mass balance while processing in an empty state considered only entering and exiting air. With granulation and drying, more factors are involved in the balance. Figure 5 shows an overview of the factors involved in the setup of a MEB for drying after TSG using a VFBD. The blue arrows show the flow path of air, whereas the black arrows show the transportation path of the granules. Water enters the drying system via the granules, inlet air and ambient air and leaves via the outlet air, with dried granules and gets lost due to fines that remain trapped in the product filter. The loss of granules ($\dot{m}_{solid-loss-OUT}$) and hence the loss of water in the granules ($\dot{m}_{w-granules-loss-OUT}$) were neglected in the further calculations. While drying, energy enters the system via heated air ($\dot{Q}_{air-IN}$), ambient air ($\dot{Q}_{ambient-air-IN}$) and granules ($\dot{Q}_{granules-IN}$) and exits the dryer through the outlet air ($\dot{Q}_{air-OUT}$), conduction of the dryer ($\dot{Q}_{conduction-OUT}$) and energy applied for evaporation ($\dot{Q}_{evaporation-OUT}$) of water from the wet granules. The energy flux during drying is presented in orange.

The stepwise derivation of the mass balance for the dryer in the empty state is demonstrated in the "Derivation of Mass Balance—Empty Dryer" section. The derivation of the mass balance during the drying of granules is shown using an exemplary timepoint from the same drying process as in the demonstration of the empty dryer only after the heating phase, where now granules of lactose-MCC formulation were dried. The process parameters used for the calculations are listed in Table 5.

Based on Fig. 5, the following mass balance for water while drying and neglecting the loss of granules through the filter can be set up as shown in Eq. (14). In addition to air, the water entering the system through the granules ($\dot{m}_{w-granules-IN}$) and water leaving the system through the dried granules ($\dot{m}_{w-granules-OUT}$) is involved in the balance. After rearranging Eq. (14) according to $\dot{m}_{w-granules-OUT}$, the LOD can be calculated.

$$\begin{aligned}&\dot{m}_{w-IN} + \dot{m}_{w-ambient-IN} + \dot{m}_{w-granules-IN}\\&= \dot{m}_{w-OUT} + \dot{m}_{w-corr.} + \dot{m}_{w-granules-OUT}\end{aligned} \tag{14}$$

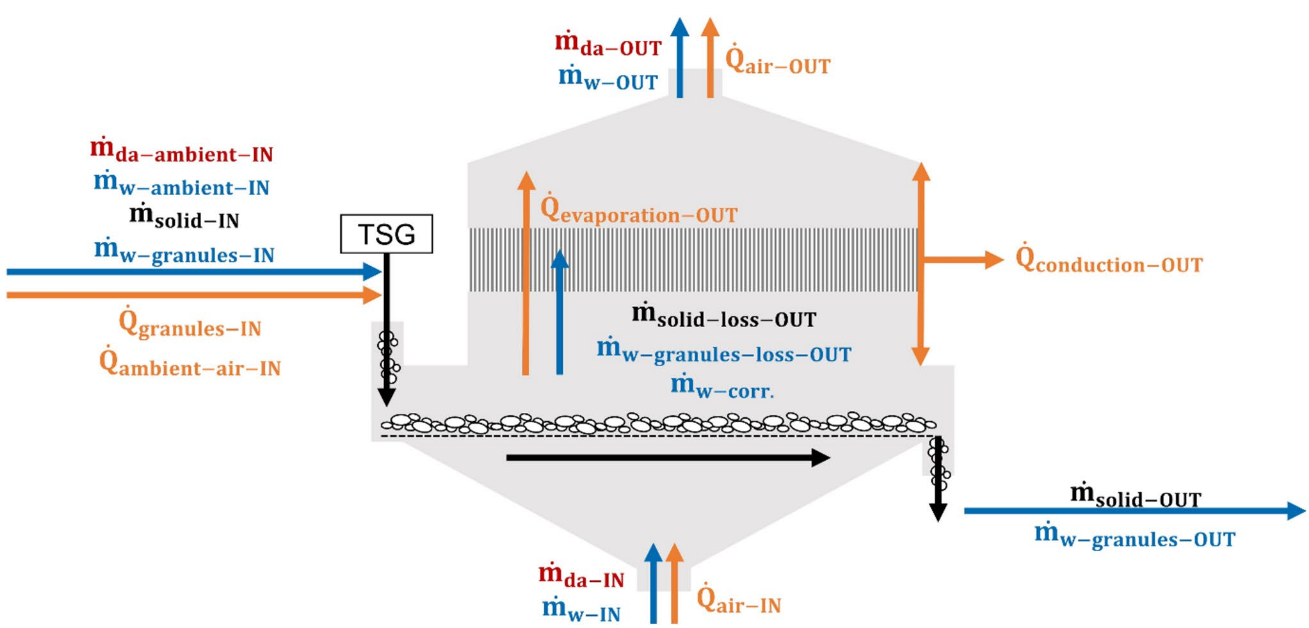


**Fig. 5** Overview of factors involved in the MEB during drying via VFBD

**Table 5** Process parameters used for the demonstrating the MEB derivation at a certain time point during drying and granulation of the lactose-MCC formulation

| Process parameter | Value at *t* |
|---|---|
| $AF_{IN}$ | 18.01 $Nm^3/h$ |
| $T_{compressedair}$ | 298.95 K |
| $\varphi_{IN}$ | 4.88% |
| $X_{IN}$ | 0.985 g/kg |
| $p_{IN}$ | 1026.5 hPa |
| $T_{IN}$ | 321.15 K |
| $T_{OUT}$ | 298.45 K |
| $AF_{OUT}$ | 19.03 $Nm^3/h$ |
| $T_{OUT2}$ | 300.05 K |
| $\varphi_{OUT}$ | 42.37% |
| $X_{OUT}$ | 9.389 g/kg |
| $p_{OUT}$ | 1011.5 hPa |
| $T_{ambient}$ | 298.85 K |
| $\varphi_{ambient}$ | 36.1% |
| $X_{ambient}$ | 7.40 g/kg |
| $p_{ambient}$ | 1015.0 hPa |
| $\dot{SFR}_{IN}$ | 1.196 kg/h |
| $\dot{LFR}$ | 0.24 kg/h |
| $LOD_0$ | 0.93% |
| $T_{barrel3}$ | 298.85 K |

First, the mass flow of the solid into the dryer ($\dot{m}_{solid-IN}$) is calculated by excluding the water content of the starting material ($LOD_0$) using Eq. (15):

$$\dot{m}_{solid-IN}\left[\frac{\mathrm{kg}}{\mathrm{h}}\right] = \dot{SFR} * \left(1 - \frac{LOD_0}{100}\right) \tag{15}$$

$$\dot{m}_{solid-IN} = 1.196\frac{\mathrm{kg}}{\mathrm{h}} * \left(1 - \frac{0.93\%}{100}\right) = 1.185\frac{\mathrm{kg}}{\mathrm{h}}$$

Next, the theoretical liquid mass flow entering as $\dot{m}_{w-granules-IN}$ is calculated using the $\dot{LFR}$ and $LOD_0$ according to Eq. (16):

$$\dot{m}_{w-granules-IN}\left[\frac{\mathrm{kg}}{\mathrm{h}}\right] = \dot{LFR} * \left(\frac{LOD_0}{100} * \dot{SFR}\right) \tag{16}$$

$$\dot{m}_{w-granules-IN} = 0.24\frac{\mathrm{kg}}{\mathrm{h}} * \left(\frac{0.93\%}{100} * 1.196\frac{\mathrm{kg}}{\mathrm{h}}\right) = 0.251\frac{\mathrm{kg}}{\mathrm{h}}$$

The incoming and outgoing mass of water were calculated as described in the empty state using Eqs. (4) to (10). Based on this, the calculated mass flows are as follows: $\dot{m}_{w-IN} = 0.0229\frac{\mathrm{kg}}{\mathrm{h}}$; $\dot{m}_{w-ambient-IN} = 0.0073\frac{\mathrm{kg}}{\mathrm{h}}$; $\dot{m}_{w-OUT} = 0.228\frac{\mathrm{kg}}{\mathrm{h}}$. The $\dot{m}_{W-corr.}$ is used from the heating phase of the dryer and corresponds to $0.0076\frac{\mathrm{kg}}{\mathrm{h}}$. Equation (14) was converted to $\dot{m}_{w-granules-OUT}$ and is described in Eq. (17) as follows:

$$\dot{m}_{w-granules-OUT}\left[\frac{\mathrm{kg}}{\mathrm{h}}\right] = \dot{m}_{w-IN} + \dot{m}_{w-ambient-IN} + \dot{m}_{w-granules-IN} - \dot{m}_{w-OUT} - \dot{m}_{w-corr.} \tag{17}$$

$$\dot{m}_{w-granules-OUT} = 0.0229\frac{\mathrm{kg}}{\mathrm{h}} + 0.0073\frac{\mathrm{kg}}{\mathrm{h}} + 0.251\frac{\mathrm{kg}}{\mathrm{h}} - 0.228\frac{\mathrm{kg}}{\mathrm{h}} - 0.0076\frac{\mathrm{kg}}{\mathrm{h}} = 0.0462\frac{\mathrm{kg}}{\mathrm{h}}$$

Consequently, the difference between the $\dot{m}_{w-granules-IN}$ and the $\dot{m}_{w-granules-OUT}$ corresponds to the mass flow rate of evaporating water ($\dot{m}_{w-evap-OUT}$) while drying described in Eq. (18):

$$\dot{m}_{w-evap-OUT}\left[\frac{\mathrm{kg}}{\mathrm{h}}\right] = \dot{m}_{w-granules-IN} - \dot{m}_{w-granules-OUT} \tag{18}$$

$$\dot{m}_{w-evap-OUT} = 0.251\frac{\mathrm{kg}}{\mathrm{h}} - 0.0462\frac{\mathrm{kg}}{\mathrm{h}} = 0.205\frac{\mathrm{kg}}{\mathrm{h}}$$

With the assumption that no granules are lost while drying, the inlet mass flow rate of the powder $\dot{m}_{solid-IN}$ equals the outlet mass of the dried granules ($\dot{m}_{solid-OUT}$). Equation (19) describes the calculation of the LOD.

$$LOD[\%] = \frac{\dot{m}_{w-granules-OUT}}{\dot{m}_{solid-OUT} + \dot{m}_{w-granules-OUT}} * 100 \tag{19}$$

$$LOD = \frac{0.0462\frac{\mathrm{kg}}{\mathrm{h}}}{1.185\frac{\mathrm{kg}}{\mathrm{h}} + 0.0462\frac{\mathrm{kg}}{\mathrm{h}}} * 100 = 3.75\%$$

In comparison, the measured LOD at 130 min was 3.73%, which is close to the predicted LOD for this example of 3.75%. The demonstration does not include the uncertainty of the sensors used for the prediction. Figure 6 displays the predicted and measured LOD over time, including the model uncertainty. Thereby, the prediction with uncertainty covered a range of 3–4% for the LOD over the process of 150 min. The high fluctuations reached a steady state after 90 min of processing. Thus, a higher precision of the prediction is reached at the same time when $T_{OUT2}$ also achieves equilibrium. While production, longer processing times are obtained, and thereby, higher precision of the predicted LOD is obtained. Nevertheless, the prediction via mass balance showed good agreement with the measured LOD. The measured LOD increased in certain time periods, which is also covered by the predicted LOD values. An RMSE of 0.54% was obtained.

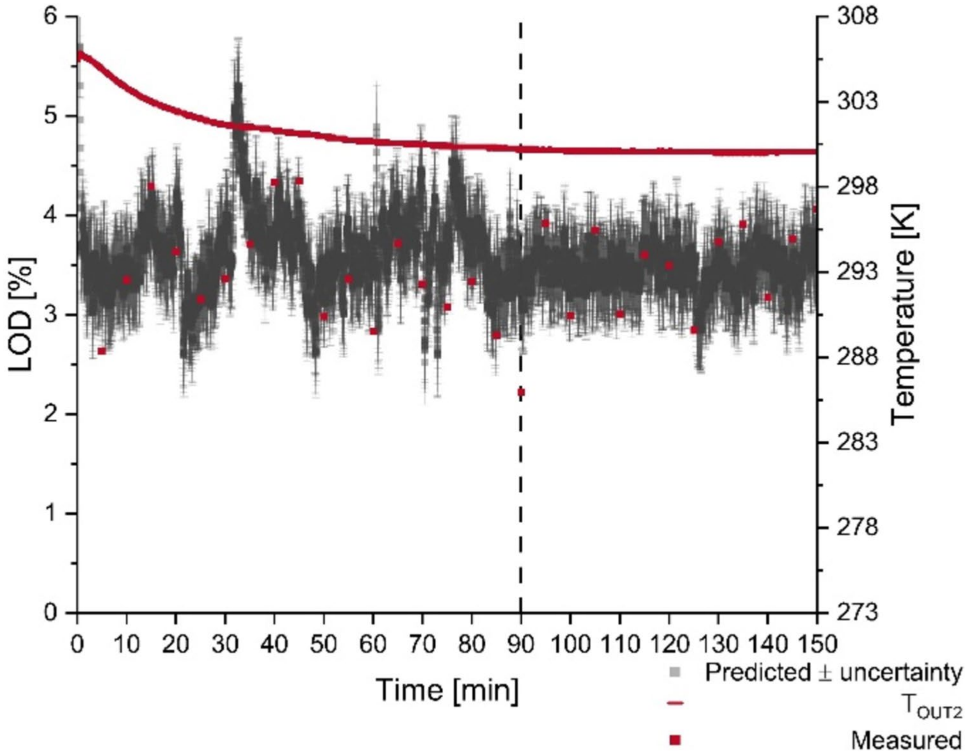


**Fig. 6** Predicted LOD with $n=1$ with 9000 measuring points, predicted ± uncertainty and measured LOD with $n=1$ over 150 min

### Prediction of LOD by Mass Balance

The application of the mass balance for prediction is displayed for the two formulations (mannitol and lactose-MCC). Each formulation was processed under three different drying conditions to cover different ranges of LOD. Figure 7 displays the prediction vs. measured LOD while drying mannitol and Fig. 8 shows the lactose-MCC with the related heating phase. The water difference through incoming and outgoing air $\dot{m}_{w-corr.}$ was determined for each run using the heating phase and is displayed in Figs. 7a and 8a. Thereby, the $\dot{m}_{w-corr.}$ showed different values and fluctuations as the experiments were not conducted on the same day except for the granulation and drying for the first and third drying process ($M1$ and $M3$). The $\dot{m}_{w-corr.}$ showed a similar value compared to the drying conditions at $M2$. The conditions of the compressed supply air cannot be controlled, which might be a reason for the different obtained $\dot{m}_{w-corr.}$ values at different drying parameters and thus days. Applying higher $T_{IN}$ or $AF_{IN}$ resulted decrease in LOD. Decreasing $Vib$ might lead to lower LOD depending on $AF_{IN}$ as the residence time of the granules is affected. The measured LOD over time lies within the predicted values (Fig. 7b). The predicted LOD showed high fluctuations, which can be attributed to the variation in absolute humidity during drying. The $X_{OUT}$ is measured at the outlet. The granules enter the drying chamber in a wet state at low temperature, and along the dryer, they are dried, and water is evaporated. The sensor itself covered all different drying stages at one position, which might explain the fluctuations in the absolute humidity of the outlet air. By changing the drying parameters from left to right (Fig. 7b), the obtained LOD decreased and the predicted LOD fluctuations decreased. The RMSE showed a smaller value and thus corresponded better at lower LOD or higher drying efficiency. While drying the mannitol granules at $M1$, the predicted LOD exhibited the highest fluctuations. It might be that the drying capacity was not high enough to remove water from the granules compared with the higher drying temperature. Thus, resulting in an uneven evaporation of the water.

Comparing Figs. 7b and 8b, drying of lactose-MCC showed a lower fluctuation of the predicted LOD values. This indicates that the fluctuation of the absolute humidity is less, and uniform drying is obtained. Drying of lactose-MCC at $L3$ showed the highest variation in the prediction of the LOD over time. In addition, the obtained $\dot{m}_{w-corr.}$ with uncertainty is the highest (Fig. 8a). At higher $T_{IN}$ and $AF_{IN}$, the uncertainty of the sensor is higher. Drying at $L1$ showed good agreement between the prediction and the measured LOD. After 45 min, a higher LOD was measured by using the mass balance. An increased LOD was also observed in the measurement. Finally, the predicted results for the two formulations using the established mass balance exhibit a good correspondence between the prediction and measured LOD.

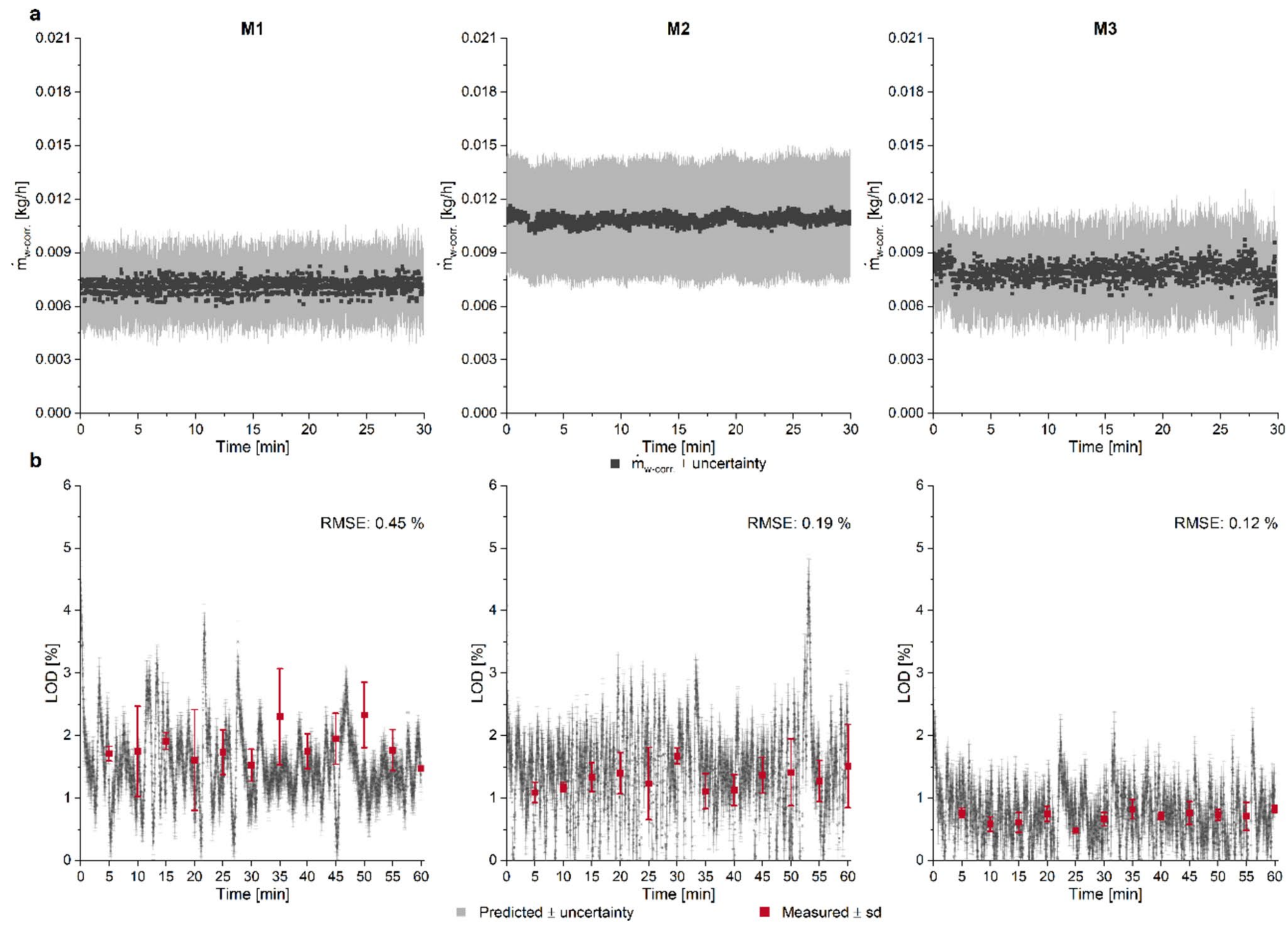


**Fig. 7** $\dot{m}_{w-corr.}$ while heating phase in empty dryer over 30 min (**a**), $n=1$ with 1800 measuring points, $\dot{m}_{w-corr} \pm$ uncertainty and LOD prediction (**b**) during drying of mannitol granules with $n=1$ with 3600 measuring points, predicted ± uncertainty and measured LOD with $n=3$, mean ± standard deviation

## Derivation of Energy Balance

### Derivation of Energy Balance—Empty Dryer

The surfaces of the VFBD consisting of stainless steel were heated via convection, resulting in additional heat loss in addition to the evaporation of water while drying. Therefore, the energy entering and leaving the system was determined. In the heating phase, the energy balance considers the ambient air, inlet air and outlet air. This estimates the heat loss due to convection and thus the heating of the dryer surfaces. The specific enthalpy of humid air or energy flux ($\dot{Q}$) is calculated according to Eq. (20) with the specific enthalpy of dry air ($h_{da}$) and water vapour ($h_{wv}$) [40].

$$\dot{Q}\left[\frac{\text{kJ}}{\text{h}}\right] = \dot{m}_{da} * h_{da} + \dot{m}_{w} * h_{wv} \tag{20}$$

The calculation of $h_{da}$ is determined using the simplified Eq. (21) using the specific heat capacity of air ($c_a$) with the value of $1.006\frac{\text{kJ}}{\text{kg*K}}$. $T$ is the temperature of the air and $T_{tr}$ is the triple point of water at 273.16K [40].

$$h_{da}\left[\frac{\text{kJ}}{\text{kg}}\right] = c_a * (T - T_{tr}) \tag{21}$$

The calculation of $h_{wv}$ is done according to Eq. (22) where $\Delta h_{wv}$ is the specific evaporation enthalpy of water at $T_{tr}$ applied with the value of $\Delta h_{wv} = 2500.9\frac{\text{kJ}}{\text{kg}}$ and $c_{wv}$ is the specific heat capacity of water vapour with $1.888\frac{\text{kJ}}{\text{kg*K}}$ [40].

$$h_{wv}\left[\frac{\text{kJ}}{\text{kg}}\right] = \Delta h_{wv} + c_{wv} * (T - T_{tr}) \tag{22}$$

According to Eqs. (20)–(22), the specific enthalpy respectively $\dot{Q}$ of the inlet, ambient and outlet air are calculated for the empty dryer as follows:

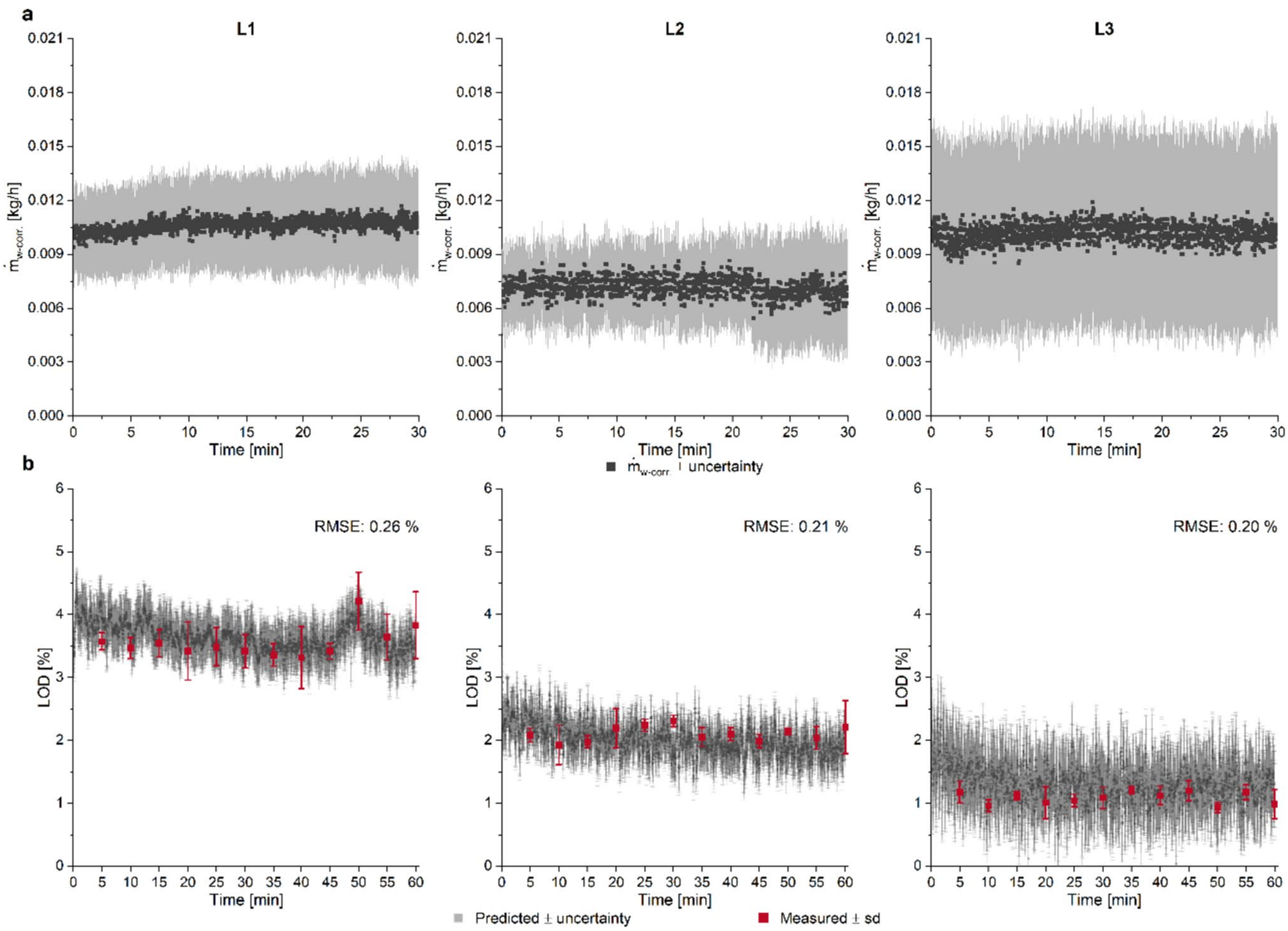


**Fig. 8** $\dot{m}_{w-corr.}$ while heating phase in empty dryer over 30 min (**a**), $n=1$ with 1800 measuring points, $\dot{m}_{w-corr} \pm$ uncertainty and LOD prediction (**b**) during drying of lactose-MCC granules with $n=1$ with 3600 measuring points, predicted ± uncertainty and measured LOD with $n=3$, mean ± standard deviation

$$\dot{Q}_{air-IN} = 23.24\frac{\mathrm{kg}}{\mathrm{h}} * 1.006\frac{\mathrm{kJ}}{\mathrm{kg} * \mathrm{K}} * (321.15 - 273.16) + \left(0.0219\frac{\mathrm{kg}}{\mathrm{h}} * \left(2500.9\frac{\mathrm{kJ}}{\mathrm{kg}} + 1.888\frac{\mathrm{kJ}}{\mathrm{kg} * \mathrm{K}} * (321.15 - 273.16)\right)\right) = 1178.7\frac{\mathrm{kJ}}{\mathrm{h}} = 327.4\ \mathrm{W}$$

$$\dot{Q}_{ambient-air-IN} = 0.27\frac{\mathrm{kg}}{\mathrm{h}} * 1.006\frac{\mathrm{kJ}}{\mathrm{kg} * \mathrm{K}} * (297.15 - 273.16) + \left(0.0021\frac{\mathrm{kg}}{\mathrm{h}} * \left(2500.9\frac{\mathrm{kJ}}{\mathrm{kg}} + 1.888\frac{\mathrm{kJ}}{\mathrm{kg} * \mathrm{K}} * (297.15 - 273.16)\right)\right) = 14.0\frac{\mathrm{kJ}}{\mathrm{h}} = 3.9\ \mathrm{W}$$

$$\dot{Q}_{air-OUT} = 23.51\frac{\text{kg}}{\text{h}} * 1.006\frac{\text{kJ}}{\text{kg} * \text{K}} * (308.15 - 273.16) + \left(0.0164\frac{\text{kg}}{\text{h}} * \left(2500.9\frac{\text{kJ}}{\text{kg}} + 1.888\frac{\text{kJ}}{\text{kg} * \text{K}} * (308.15 - 273.16)\right)\right) = 869.7\frac{\text{kJ}}{\text{h}} = 241.6\ \text{W}$$

For the heating phase, the energy balance can be calculated according to Eq. (23). The difference between the incoming and outgoing energy flux corresponds to the heat loss ($\dot{Q}_{loss}$) which is in empty dryer due to convection from the air to the dryer surface. The percentage $\dot{Q}_{loss}$ is determined according to Eq. (24) resulting 27.1% heat loss during the heating phase due to the heating of the stainless-steel parts of the drying chamber.

$$\dot{Q}_{air-IN} + \dot{Q}_{ambient-air-IN} = \dot{Q}_{air-OUT} + \dot{Q}_{loss} \tag{23}$$

$$\dot{Q}_{loss} = \left(\dot{Q}_{air-IN} + \dot{Q}_{ambient-air-IN}\right) - \dot{Q}_{air-OUT} = (327.4\ W + 3.9\ \text{W}) - 241.6\ \text{W} = 89.7\ \text{W}$$

$$\dot{Q}_{loss}[\%] = \frac{\dot{Q}_{loss}}{\dot{Q}_{air-IN} + \dot{Q}_{ambient-air-IN}} * 100 \tag{24}$$

$$\dot{Q}_{loss}[\%] = \frac{89.7\ \text{W}}{327.4\ \text{W} + 3.9\ \text{W}} * 100 = 27.1\%$$

### Derivation of Energy Balance—Drying of Granules

In addition to the air, granules entering and leaving the drying system at a certain temperature are included to set the energy balance in Eq. (23) resulting in Eq. (25). The wet and dried granules consist of a specific enthalpy, which is calculated using Eq. (26). The specific heat capacity of each formulation was determined using differential scanning calorimetry and resulted for lactose-MCC in $c_{lactose-MCC} = 1.841\frac{\text{kJ}}{\text{kg*K}}$ and for mannitol in $c_{mannitol} = 1.758\frac{\text{kJ}}{\text{kg*K}}$. $c_w$ is the specific heat capacity of water with a value of $4.22\frac{\text{kJ}}{\text{kg*K}}$.

$$\dot{Q}_{air-IN} + \dot{Q}_{ambient-air-IN} + \dot{Q}_{granules-IN} = \dot{Q}_{air-OUT} + \dot{Q}_{granules-OUT} + \dot{Q}_{loss} \tag{25}$$

$$\dot{Q}_{granules} = \dot{m}_{solid} * c_{formulation} * \left(T - T_{tr}\right) + \dot{m}_{w-granules} * c_w * \left(T - T_{tr}\right) \tag{26}$$

For the entering granules, the $T_{barrel3}$ is used as the temperature, and for the leaving granules the temperature $T_{granules}$ is predicted according to Eq. (5). Thus, the energy flux of the granules is determined as follows:

$$T_{granules} = -0.87 * 18.01\frac{\text{Nm}}{\text{h}} + 2.00 * 298.45\ \text{K} - 282.87 = 298.36\ \text{K}$$

$$\dot{Q}_{granules-IN} = 1.185\frac{\text{kg}}{\text{h}} * 1.841\frac{\text{kJ}}{\text{kg} * \text{K}} * (298.85\ \text{K} - 273.16\ \text{K}) + 0.251\frac{\text{kg}}{\text{h}} * 4.22\frac{\text{kJ}}{\text{kg} * \text{K}} * (298.85\ \text{K} - 273.16\ \text{K}) = 83.26\frac{\text{kJ}}{\text{h}} = 23.1\ \text{W}$$

$$\dot{Q}_{granules-OUT} = 1.185\frac{\text{kg}}{\text{h}} * 1.841\frac{\text{kJ}}{\text{kg} * \text{K}} * (298.36\,\text{K} - 273.16\,\text{K}) + 0.0462\frac{\text{kg}}{\text{h}} * 4.22\frac{\text{kJ}}{\text{kg} * \text{K}} * (298.36\,\text{K} - 273.16\,\text{K}) = 59.89\frac{\text{kJ}}{\text{h}} = 16.6\,\text{W}$$

The energy flux of the air while drying is calculated as for the heating phase and resulted in the example in $\dot{Q}_{air-IN} = 328.1$ W, $\dot{Q}_{ambient-air-IN} = 12.3$ W and

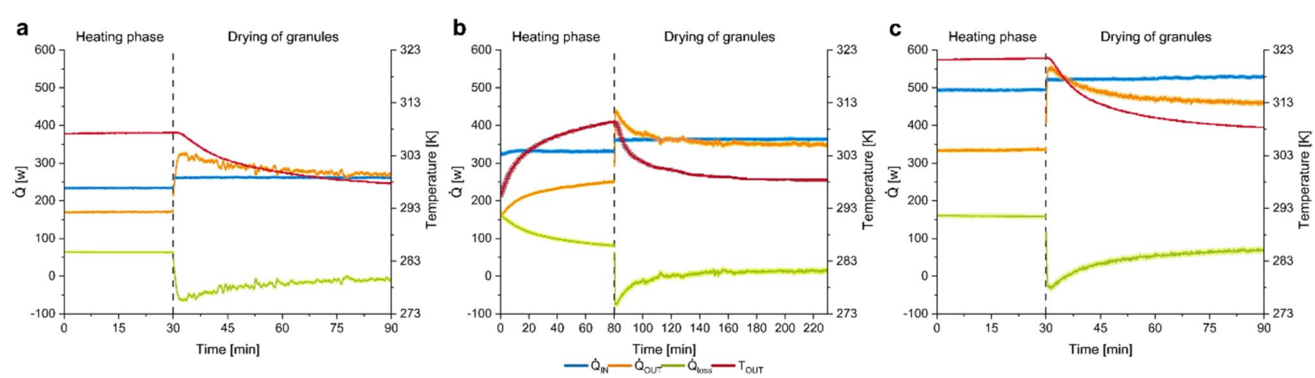


**Fig. 9** Q̇ of incoming and leaving energy, $\dot{Q}_{loss}$ and $T_{OUT}$ during the heating phase and drying at M1 (**a**), L1 condition with longer time (**b**) and L3 (**c**), $n = 1$, value ± uncertainty

**Table 6** $\dot{Q}$ of incoming and leaving energy in [W], $\dot{Q}_{loss}$ [%] and $T_{OUT}$ [K] during the heating phase and drying of mannitol granules under different drying conditions, $n = 1$ with 300 measuring points (heating phase) and 600 measuring points (drying of granules), mean ± uncertainty

| Experiment | Heating phase | | | | Drying of granules | | | |
|---|---|---|---|---|---|---|---|---|
| | $\dot{Q}_{IN}$ | $\dot{Q}_{OUT}$ | $\dot{Q}_{loss}$ | $T_{OUT}$ | $\dot{Q}_{IN}$ | $\dot{Q}_{OUT}$ | $\dot{Q}_{loss}$ | $T_{OUT}$ |
| ***M1*** | 234.1 ± 2.3 | 170.4 ± 2.0 | 27.2 ± 1.3 | 307.3 | 261.5 ± 2.6 | 270.3 ± 3.1 | −3.4 ± 1.6 | 297.9 |
| ***M2*** | 342.9 ± 2.8 | 257.8 ± 3.0 | 24.8 ± 1.2 | 309.1 | 370.0 ± 3.1 | 347.4 ± 4.0 | 6.1 ± 1.4 | 300.9 |
| ***M3*** | 353.1 ± 2.8 | 232.0 ± 2.7 | 34.3 ± 1.1 | 311.4 | 380.5 ± 3.2 | 341.4 ± 3.9 | 10.3 ± 1.3 | 303.2 |

$\dot{Q}_{air-OUT} = 332.3$ W. Thus, the $\dot{Q}_{loss}$ is determined by converting Eq. (25):

$$\dot{Q}_{loss} = 328.1\ \text{W} + 12.3\ \text{W} + 23.1\ \text{W} - 332.3\ \text{W} - 16.6\ \text{W} = 14.6\ \text{W}$$

$$\dot{Q}_{loss} = \frac{14.6\ \text{W}}{(328.1\ \text{W} + 12.3\ \text{W} + 23.1\ \text{W})} * 100 = 4.02\%$$

$\dot{Q}_{IN}$, $\dot{Q}_{OUT}$ and $\dot{Q}_{loss}$ are calculated over time for the heating phase and drying of the granules displayed in Fig. 9. $\dot{Q}_{IN}$ and $\dot{Q}_{OUT}$ represent the sum of the entering, respectively, leaving $\dot{Q}$. Figure 9b shows the energy balance over a longer drying time for the same experiment used for the stepwise deviation of the MEB. The heating phase includes the complete heating of the system (Fig. 9b). During the heating phase, the $T_{OUT}$ increases and thus the $\dot{Q}_{OUT}$. The lower the temperature difference between $T_{IN}$ and $T_{OUT}$, the lower $\dot{Q}_{loss}$ as $\dot{Q}_{OUT}$ becomes higher. During this phase, the entire device is heated, including the sieve plate and dryer walls (Fig. 9b). For experiments shown in Fig. 9a and c, the system was already heated as previous runs were conducted before indicating constant values for $\dot{Q}_{IN}$, $\dot{Q}_{OUT}$, $T_{OUT}$ and $\dot{Q}_{loss}$. As soon as wet granules enter the drying chamber, $T_{OUT}$ is decreasing as water evaporates and the granules are dried. In addition, the pipes were heated up and it takes time till the $T_{OUT}$ is reaching an equilibrium. At the beginning of drying, $\dot{Q}_{loss}$ is low because the granules are also dried by the heated surfaces via conduction. As the surfaces are cooled down over time, the $\dot{Q}_{OUT}$ is decreasing as the temperature of the exhaust air reduces and thus the $\dot{Q}_{loss}$ is increasing. Nevertheless, the $\dot{Q}_{loss}$ is lower during drying compared to the heating phase. $\dot{Q}_{OUT}$ especially the $\dot{Q}_{air-OUT}$ is higher during drying because it also consists of the evaporated water and thus more energy.

The energy flux rates $\dot{Q}$ for the different drying conditions are summarised for the drying of mannitol granules in Table 6 and lactose-MCC granules in Table 7. For the shown drying processes, the $\dot{Q}_{loss}$ is around 30% due to conduction through the dryer walls and the sieve plate. The heating phase for mannitol granules (Table 6) showed a slightly lower $\dot{Q}_{loss}$ by drying at higher air flow, indicating that the walls were not equally heated. The higher the evaporated amount of water, the higher the $\dot{Q}_{loss}$ while drying the granules. During the drying of mannitol granules at $M1$ drying conditions, a negative $\dot{Q}_{loss}$ was observed. The change of $\dot{Q}_{IN}$ and $\dot{Q}_{OUT}$ is shown in Fig. 9a, where it is observed that $T_{OUT}$ is not reaching an equilibrium through 1 h of drying. $\dot{Q}_{IN}$ is therefore lower compared to $\dot{Q}_{OUT}$ resulting in a negative $\dot{Q}_{loss}$. A higher $AF_{IN}$ was used for drying in Fig. 9b compared to Fig. 9a, which might be the reason for the difference. Higher $AF_{IN}$ improved the heat distribution and resulted in an earlier onset of temperature equilibrium. $\dot{Q}_{loss}$ is less during drying of granules compared to the heating because the walls of the dryer are cooled down due to evaporation cooling. Increasing $T_{IN}$ or $AF_{IN}$, the $\dot{Q}_{IN}$ which is entering the system also increases. $\dot{Q}_{IN}$ is also dependent on the absolute humidity of the pressured air, which is not controlled. In a previous publication [21], the second drying stage was reached earlier with a lower LOD and the obtained $T_{OUT}$ is also higher, as shown in Tables 6 and 7.

Based on the literature, the $\dot{Q}_{loss}$ is only defined by the difference in $\dot{Q}_{IN}$ and $\dot{Q}_{OUT}$. Mortier et al. [26] defined the total required energy during drying as the sum of energy needed for evaporation of water from the wet granules as well as for heating the wet granules, the energy loss through

**Table 7** $\dot{Q}$ of incoming and leaving energy in [W], $\dot{Q}_{loss}$ [%] and $T_{OUT}$ [K] during the heating phase and drying of lactose-MCC granules under different drying conditions, $n = 1$ with 300 measuring points (heating phase) and 600 measuring points (drying of granules), mean ± uncertainty

| Experiment | Heating phase | | | | Drying of granules | | | |
|---|---|---|---|---|---|---|---|---|
| | $\dot{Q}_{IN}$ | $\dot{Q}_{OUT}$ | $\dot{Q}_{loss}$ | $T_{OUT}$ | $\dot{Q}_{IN}$ | $\dot{Q}_{OUT}$ | $\dot{Q}_{loss}$ | $T_{OUT}$ |
| ***L1*** | 339.7 ± 2.8 | 231.4 ± 2.7 | 31.9 ± 1.1 | 305.5 | 368.3 ± 3.3 | 352.1 ± 4.1 | 4.4 ± 1.4 | 298.0 |
| ***L2*** | 346.0 ± 2.7 | 229.8 ± 2.7 | 33.6 ± 1.1 | 312.3 | 376.1 ± 3.2 | 358.8 ± 4.2 | 4.6 ± 1.4 | 300.9 |
| ***L3*** | 493.7 ± 3.8 | 334.1 ± 3.9 | 32.3 ± 1.1 | 321.3 | 528.8 ± 4.0 | 460.5 ± 5.3 | 12.9 ± 1.3 | 308.5 |

the dryer walls and due to passing the filter. This consideration took more parameters into account. Unfortunately, no $\dot{Q}_{loss}$ or required energy was displayed, which might be used for comparison.

## Conclusion

The derived MEB can predict the LOD based on the logged data of QbCon® 1 without additional sensors. This approach is another option for predicting the LOD besides the established ones via grey box modelling by Elkhashap et al. [33, 41] or mechanistic modelling implemented by Wikström et al. [35] for the production scale VFBD of QbCon® 25. In the empty state, the measured amount of water leaving the system is lower than the amount of water entering through the air. No explanation for this observation was found. However, this was already observed for the segmented dryer of ConsiGma™ [26]. The included sensor uncertainty increased at higher $T_{IN}$, especially in the empty state. The precision of the sensors is limited. Therefore, the difference of water entering and leaving the system in the empty state needs to be considered in the mass balance of drying of granules. Hence, data from the heating phase in the empty state are required for predicting LOD. With this assumption, a good correlation was observed for the drying of the two different formulations. Various drying conditions were investigated to cover different LOD values, which were predictable in all cases. Thus, the mass balance might be useful as a soft sensor so-called trivial observer to predict LOD in-line based on the logged process parameters of the machine. Advantages of the mass balance approach are the use of already installed sensors without additional acquisition of sensors, e.g. NIRS, to implement a PAT method. Additionally, mass balance offers the possibility of being used as an orthogonal method to monitor the LOD independent of a PAT method to lower the risk of failure during the adaption of process parameters if one method detects an out-of-range LOD. It must be considered that the mass balance alone cannot be used to adjust the process parameter to obtain a desired LOD, which is a disadvantage of this approach. The implemented energy balance showed that the heat loss in empty state based on convection is around 30% because of the heating of stainless-steel walls. While drying granules, the heat loss is lower by up to 10% depending on the applied drying conditions. When the wet granules enter the drying chamber, the heat loss is lower as the heated wall contributes to the required evaporation of water. The derived energy balance might be used to determine whether the system can expend the energy required to dry to a desired LOD. Compared to the established energy balances in the literature for several drying systems [24, 26, 42], this study provides values for the heat loss during the heating phase and drying of granules, thus provides a good insight into the energy flux.

**Acknowledgements** The authors thank Silvia Wöltje for her help in the determination of absolute humidity, Dr. Robin Meier, Daniel Emanuele and Stefan Klinken for their constructive feedback, Andrea Michel for carrying out the dynamic scanning calorimetry measurement, Meggle for providing Granulac® 200 and Martin Lück for the support during the experiments and feedback on an earlier version of the manuscript.

**Author Contribution** Conceptualization: K. K., P. K.; methodology: K. K., F. H., A. A., P. K.; formal analysis and investigation: K. K., F. H.; writing—original draft preparation: K. K., F. H.; writing—review and editing: A. A., P. K.; supervision: P. K.

**Funding** Open Access funding enabled and organized by Projekt DEAL.

**Data Availability** Data will be made available on request.

## Declarations

**Competing of Interest** The authors declare no competing interests.

**Financial Interest** Katharina Kiricenko and Peter Kleinebudde declare they have no financial interests. Felix Hartmann and Andreas Altmeyer are employed by L.B. Bohle Maschinen und Verfahren GmbH.



## References

1. Keleb EI, Vermeire A, Vervaet C, Remon JP. Twin screw granulation as a simple and efficient tool for continuous wet granulation. Int J Pharm. 2004;273:183–94. https://doi.org/10.1016/j.ijpharm.2004.01.001.
2. Dhenge RM, Fyles RS, Cartwright JJ, Doughty DG, Hounslow MJ, Salman AD. Twin screw wet granulation: granule properties. Chem Eng J. 2010;164:322–9. https://doi.org/10.1016/j.cej.2010.05.023.
3. Vercruysse J, Córdoba Díaz D, Peeters E, Fonteyne M, Delaet U, Van Assche I, De Beer T, Remon JP, Vervaet C. Continuous twin screw granulation: influence of process variables on granule and tablet quality. Eur J Pharm Biopharm. 2012;82:205–11. https://doi.org/10.1016/j.ejpb.2012.05.010.
4. Vanhoorne V, Vanbillemont B, Vercruysse J, De Leersnyder F, Gomes P, De Beer T, Remon JP, Vervaet C. Development of a controlled release formulation by continuous twin screw

granulation: influence of process and formulation parameters. Int J Pharm. 2016;505:61–8. https://doi.org/10.1016/j.ijpharm.2016.03.058.
5. Meier R, Thommes M, Rasenack N, Moll KP, Krumme M, Kleinebudde P. Granule size distributions after twin-screw granulation - do not forget the feeding systems. Eur J Pharm Biopharm. 2016;106:59–69. https://doi.org/10.1016/j.ejpb.2016.05.011.
6. Djuric D, Kleinebudde P. Continuous granulation with a twin-screw extruder: impact of material throughput. Pharm Dev Technol. 2010;15:518–25. https://doi.org/10.3109/10837450903397578.
7. Franke M, Riedel T, Meier R, Schmidt C, Kleinebudde P. Comparison of scale-up strategies in twin-screw wet granulation. Int J Pharm. 2023;641: 123052. https://doi.org/10.1016/j.ijpharm.2023.123052.
8. Meier R, Moll KP, Krumme M, Kleinebudde P. Impact of fill-level in twin-screw granulation on critical quality attributes of granules and tablets. Eur J Pharm Biopharm. 2017;115:102–12. https://doi.org/10.1016/j.ejpb.2017.02.010.
9. Osorio JG, Sayin R, Kalbag AV, Litster JD, Martinez-Marcos L, Lamprou DA, Halbert GW. Scaling of continuous twin screw wet granulation. AIChE J. 2017;63:921–32. https://doi.org/10.1002/aic.15459.
10. Meng W, Román-Ospino AD, Panikar SS, O'Callaghan C, Gilliam SJ, Ramachandran R, Muzzio FJ. Advanced process design and understanding of continuous twin-screw granulation via implementation of in-line process analytical technologies. Adv Powder Techn. 2019;30:879–94. https://doi.org/10.1016/j.apt.2019.01.017.
11. Kumar A, Dhondt J, De Leersnyder F, Vercruysse J, Vanhoorne V, Vervaet C, Remon JP, Gernaey KV, De Beer T, Nopens I. Evaluation of an in-line particle imaging tool for monitoring twin-screw granulation performance. Powder Technol. 2015;285:80–7. https://doi.org/10.1016/j.powtec.2015.05.031.
12. Vercruysse J, Burggraeve A, Fonteyne M, Cappuyns P, Delaet U, Van Assche I, De Beer T, Remon JP, Vervaet C. Impact of screw configuration on the particle size distribution of granules produced by twin screw granulation. Int J Pharm. 2015;479:171–80. https://doi.org/10.1016/j.ijpharm.2014.12.071.
13. Plumb K. Continuous processing in the pharmaceutical industry. Chem Eng Res Des. 2005;83:730–8. https://doi.org/10.1205/cherd.04359.
14. Singh M, Shirazian S, Ranade V, Walker GM, Kumar A. Challenges and opportunities in modelling wet granulation in pharmaceutical industry – a critical review. Powder Technol. 2022;403: 117380. https://doi.org/10.1016/j.powtec.2022.117380.
15. Vercruysse J, Peeters E, Fonteyne M, Cappuyns P, Delaet U, Van Assche I, De Beer T, Remon JP, Vervaet C. Use of a continuous twin screw granulation and drying system during formulation development and process optimization. Eur J Pharm Biopharm. 2015;89:239–47. https://doi.org/10.1016/j.ejpb.2014.12.017.
16. Pauli V, Elbaz F, Kleinebudde P, Krumme M. Methodology for a variable rate control strategy development in continuous manufacturing applied to twin-screw wet-granulation and continuous fluid-bed drying. J Pharm Innov. 2018;13:247–60. https://doi.org/10.1007/s12247-018-9320-6.
17. Monaco D, Omar C, Reynolds GK, Tajarobi P, Litster JD, Salman AD. Drying in a continuous wet granulation line: investigation of different end of drying control methods. Powder Technol. 2021;392:157–66. https://doi.org/10.1016/j.powtec.2021.07.004.
18. Menth J, Maus M, Wagner KG. Continuous twin screw granulation and fluid bed drying: a mechanistic scaling approach focusing optimal tablet properties. Int J Pharm. 2020;586: 119509. https://doi.org/10.1016/j.ijpharm.2020.119509.
19. Zhang Y, Abatzoglou N, Hudon S, Lapointe-Garant PP, Simard JS. Dynamics of heat-sensitive pharmaceutical granules dried in a horizontal fluidized bed combined with a screw conveyor. Chem Eng Process: Process Intensif. 2021;167: 108516. https://doi.org/10.1016/j.cep.2021.108516.
20. Meier R, Emanuele D, Harbaum P. Important elements in continuous granule drying processes. TechnoPharm. 2020;10:92–101.
21. Kiricenko K, Kleinebudde P. Drying behavior of a horizontal vibrated fluidized bed dryer for continuous manufacturing. Pharm Dev Technol. 2023;28:440–51. https://doi.org/10.1080/10837450.2023.2205932.
22. Chavez PF, Stauffer F, Eeckman F, Bostijn N, Didion D, Schaefer C, Yang H, El Aalamat Y, Lories X, Warman M, Mathieu B, Mantanus J. Control strategy definition for a drug product continuous wet granulation process: industrial case study. Int J Pharm. 2022;624: 121970. https://doi.org/10.1016/j.ijpharm.2022.121970.
23. Buschmuller C, Wiedey W, Doscher C, Dressler J, Breitkreutz J. In-line monitoring of granule moisture in fluidized-bed dryers using microwave resonance technology. Eur J Pharm Biopharm. 2008;69:380–7. https://doi.org/10.1016/j.ejpb.2007.09.014.
24. Pauli V, Elbaz F, Kleinebudde P, Krumme M. Orthogonal redundant monitoring of a new continuous fluid-bed dryer for pharmaceutical processing by means of mass and energy balance calculations and spectroscopic techniques. J Pharm Sci. 2019;108:2041–55. https://doi.org/10.1016/j.xphs.2018.12.028.
25. Fonteyne M, Gildemyn D, Peeters E, Mortier STFC, Vercruysse J, Gernaey KV, Vervaet C, Remon JP, Nopens I, De Beer T. Moisture and drug solid-state monitoring during a continuous drying process using empirical and mass balance models. Eur J Pharm Biophar. 2014;87:616–28. https://doi.org/10.1016/j.ejpb.2014.02.015.
26. Mortier STFC, Gernaey KV, De Beer T, Nopens I. Analysing drying unit performance in a continuous pharmaceutical manufacturing line by means of mass–energy balances. Eur J Pharm Biopharm. 2014;86:532–43. https://doi.org/10.1016/j.ejpb.2013.12.014.
27. Temple SJ, van Boxtel AJB. Modelling of fluidized-bed drying of black tea. J Agric Eng Res. 1999;74:203–12. https://doi.org/10.1006/jaer.1999.0454.
28. Picado A, Martínez J. Mathematical modeling of a continuous vibrating fluidized bed dryer for grain. Dry Technol. 2012;30:1469–81. https://doi.org/10.1080/07373937.2012.690123.
29. Zhang Y, Abatzoglou N. Modelling of continuous drying of heat-sensitive pharmaceutical granules in a horizontal fluidised bed dryer combined with a screw conveyor at steady state. Chem Eng Sci. 2022;255: 117678. https://doi.org/10.1016/j.ces.2022.117678.
30. Rehrl J, Sacher S, Horn M, Khinast J. End-point prediction of granule moisture in a ConsiGma-25 segmented fluid bed dryer. Pharmaceutics. 2020;12:452. https://doi.org/10.3390/pharmaceutics12050452.
31. Ghijs M, Schäfer E, Kumar A, Cappuyns P, Van Assche I, De Leersnyder F, Vanhoorne V, De Beer T, Nopens I. Modeling of semicontinuous fluid bed drying of pharmaceutical granules with respect to granule size. J Pharm Sci. 2019;108:2094–101. https://doi.org/10.1016/j.xphs.2019.01.013.
32. Destro F, Salmon AJ, Facco P, Pantelides CC, Bezzo F, Barolo M. Monitoring a segmented fluid bed dryer by hybrid data-driven/knowledge-driven modeling. IFAC-PapersOnLine. 2020;53:11638–43. https://doi.org/10.1016/j.ifacol.2020.12.646.
33. Elkhashap A, Meier R, Abel D. Modeling and control of a continuous vibrated fluidized bed dryer in pharmaceutical tablets production. Pharm Ind. 2019;81:1693–700.

34. Lehmann SE, Buchholz M, Jongsma A, Innings F, Heinrich S. Modeling and flowsheet simulation of vibrated fluidized bed dryers. Processes. 2020;9:52. https://doi.org/10.3390/pr9010052.
35. Wikstrom H, Martin de Juan L, Remmelgas J, Meier R, Altmeyer S, Emanuele A, Jormanainen M, Juppo A, Tajarobi P. Drying capacity of a continuous vibrated fluid bed dryer - statistical and mechanistic model development. Int J Pharm. 2023;645:123368. https://doi.org/10.1016/j.ijpharm.2023.123368.
36. Myers RH, Montgomery DC, Anderson-Cook C. Response surface methodology: process and product optimization using designed experiments. 4th ed. Hoboken: John Wiley & Sons; 2016.
37. V VAISALA. Humidity conversions: formulas and methods for calculating humidity parameters (B210973EN-K). In: Vaisala. 2021. VIM-GLO-IND-Humidity-conversion-formulas-Technical-eBook-B210973EN-K.pdf. Accessed 15 June 2023.
38. Willmott CJ. Some comments on the evaluation of model performance. Bull Am Meteorol Soc. 1982;63:1309–13. https://doi.org/10.1175/1520-0477(1982)063%3c1309:SCOTEO%3e2.0.CO;2.
39. Davis RA. Practical numerical methods for chemical engineers: using Excel with VBA. 4th ed. Independently published; 2018.
40. Baehr HD, Kabelac S. Thermodynamik. Berlin: Springer Vieweg; 2016.
41. Elkhashap A, Meier R, Abel D. A grey box distributed parameter model for a continuous vibrated fluidized bed dryer in pharmaceutical manufacturing. 2020 European Control Conference (ECC), St. Petersburg, Russia. 2020;1415–1421. https://doi.org/10.23919/ECC51009.2020.9143770.
42. Lu M, Kranz P, Salmon A, Wilkinson S, Sibanc R. Heat transfer model and soft sensing for segmented fluidized bed dryer. Processes. 2022;10:2609. https://doi.org/10.3390/pr10122609.